

Figure S1

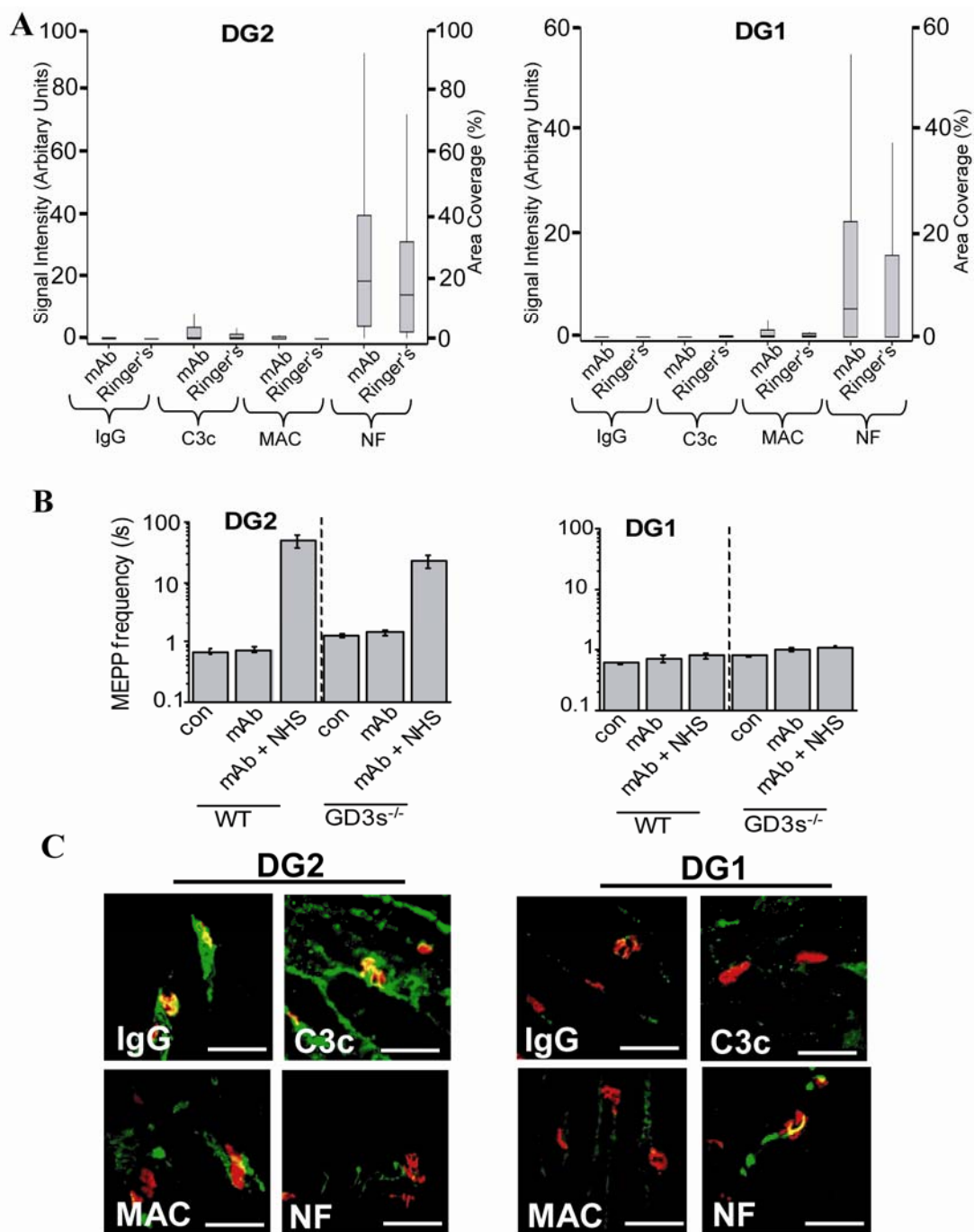


Figure S2

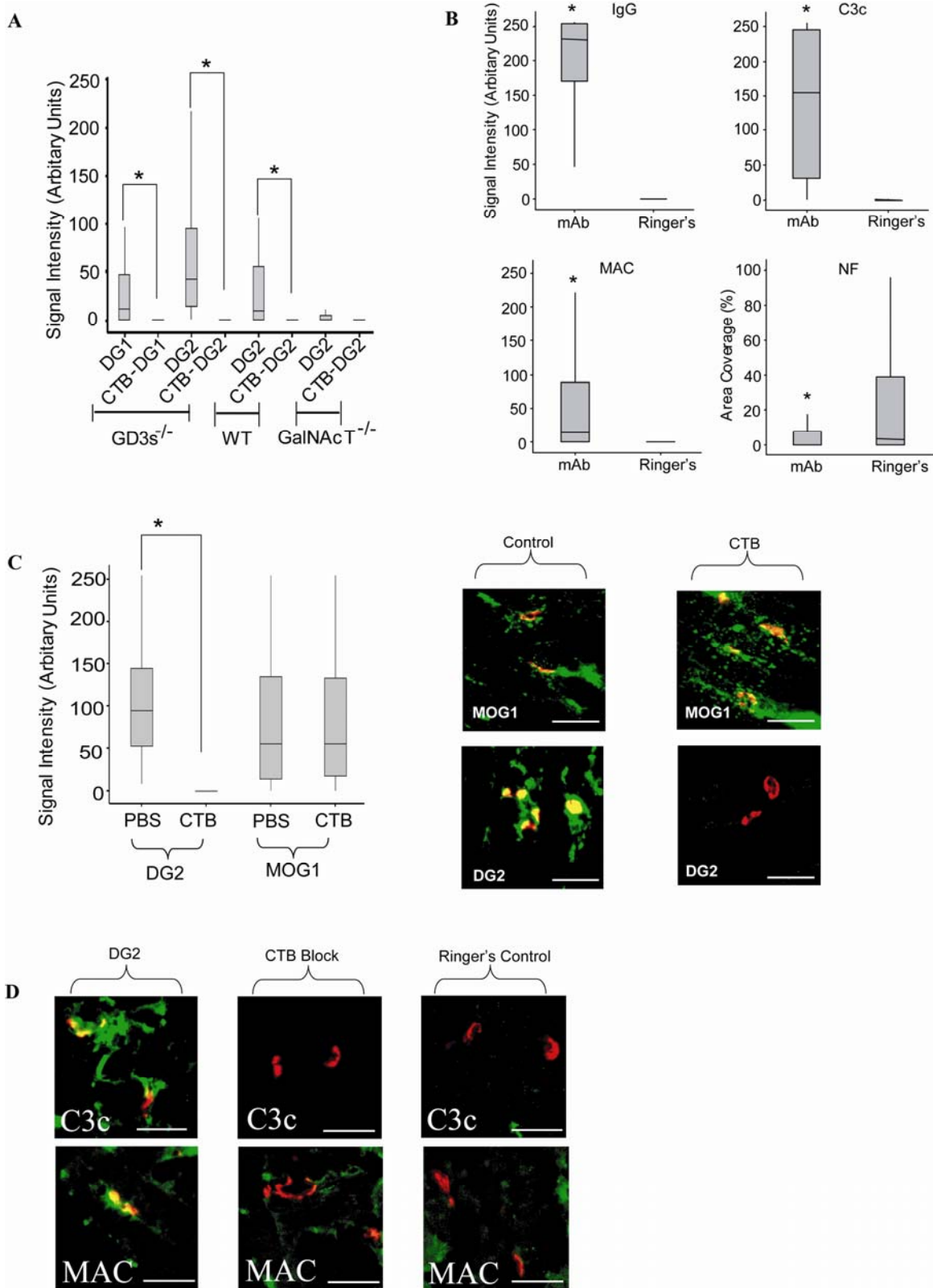


Figure S3

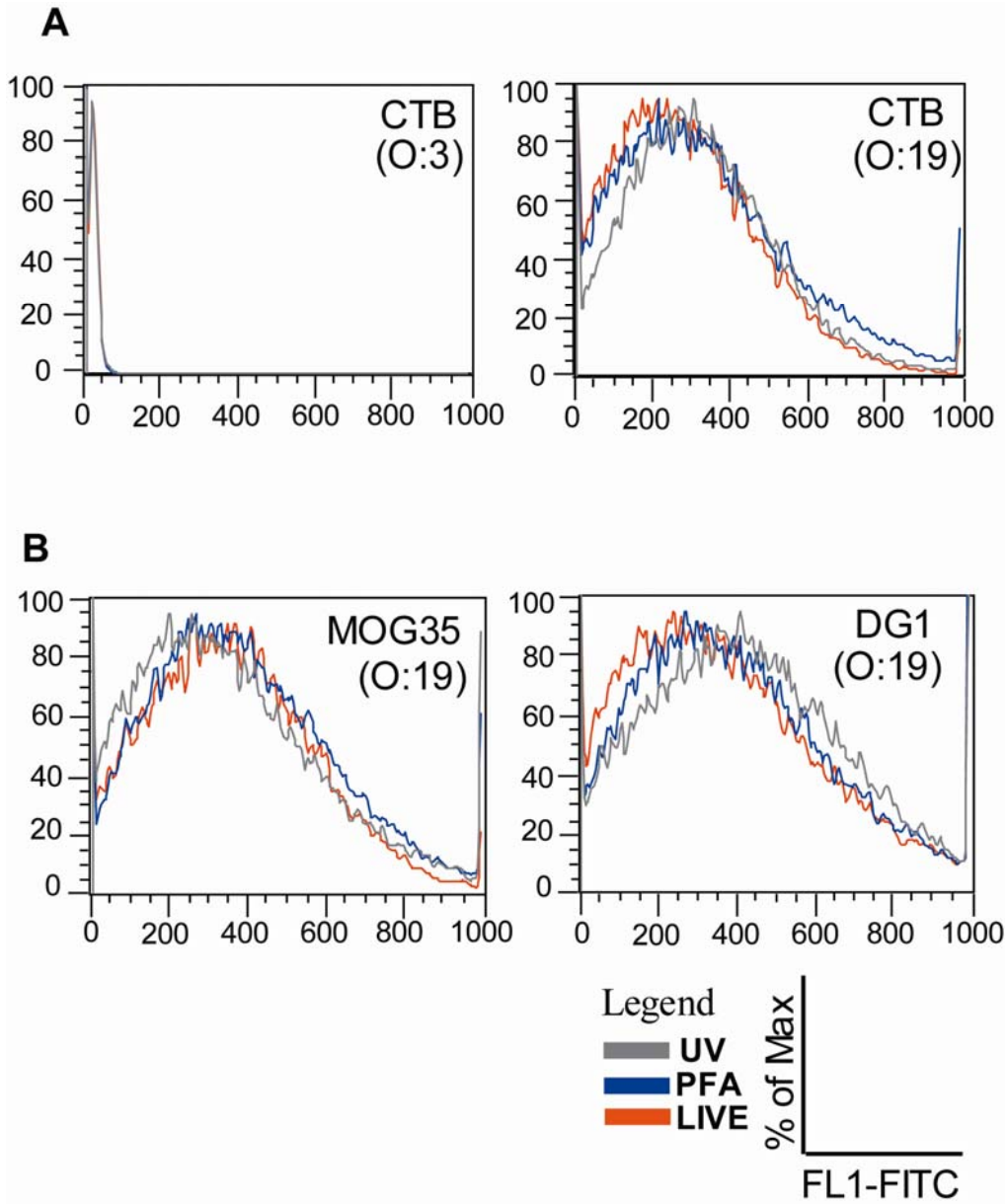


Figure S4

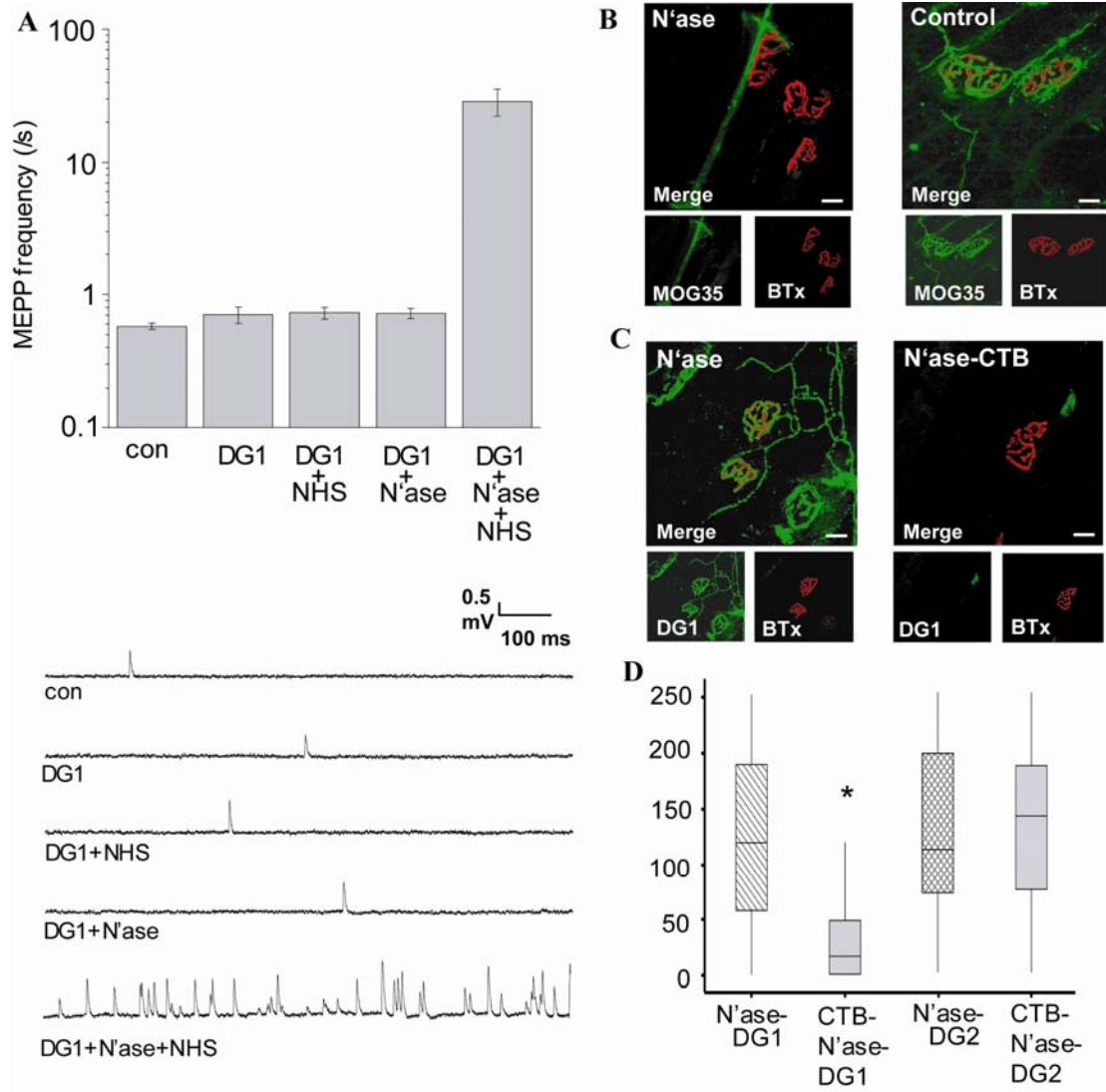


Figure S5

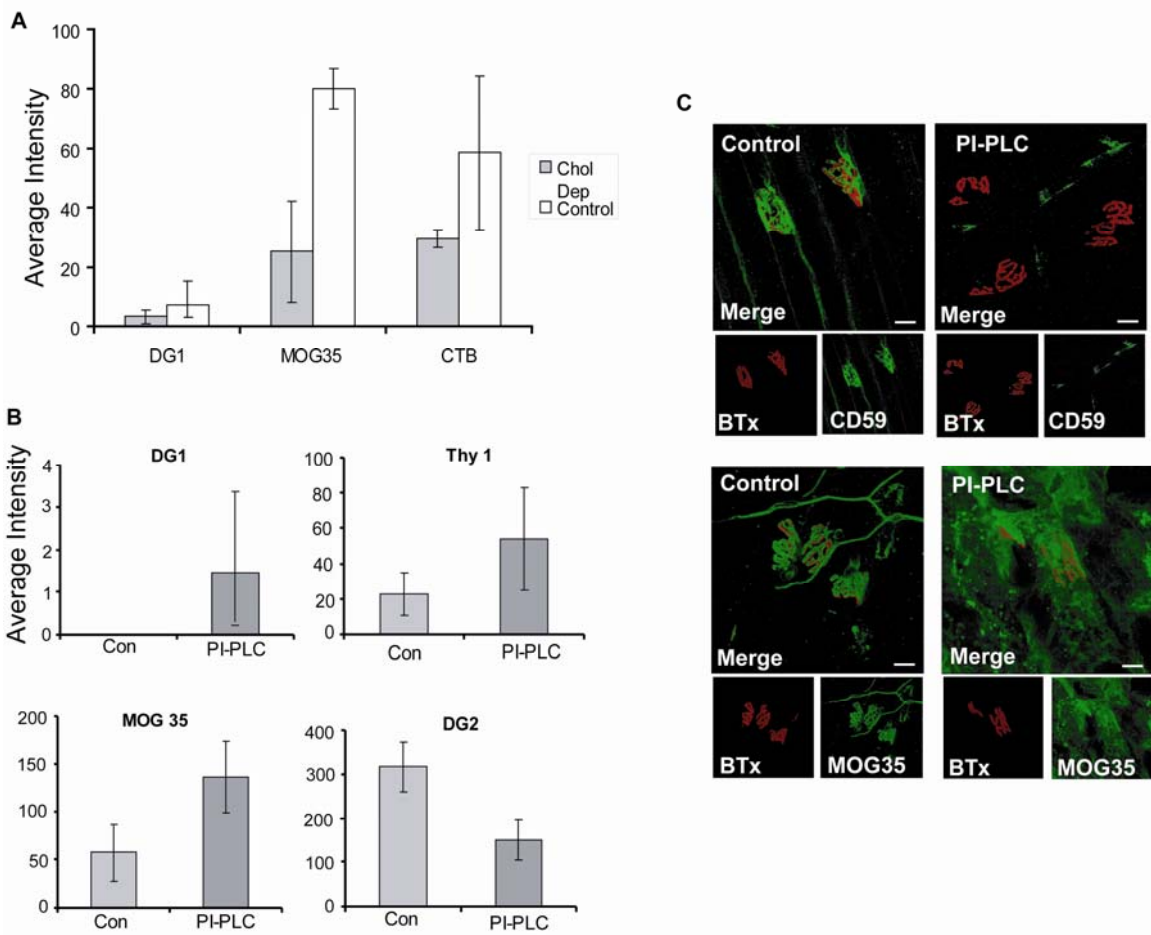


Figure S6

## SUPPLEMENTARY FIGURE LEGENDS

### Figure S1

Biosynthetic pathway for gangliosides showing activity of *GalNAcT* and *GD3s* and the structures of the major gangliosides. Ganglioside nomenclature is according to Svennerholm (1). WT mice contain the biosynthetic machinery for all potential gangliosides. *GalNAcT*<sup>-/-</sup> mice lack the *GalNAcT* gene, which results in the absence of all the gangliosides within the dotted rectangle, with retention of GM3, GD3 and GT3 only. *GD3s*<sup>-/-</sup> mice lack the *GD3s* gene, which results in the absence of all the gangliosides within the dashed rectangle (b- and c-series).

NeuAc: neuraminic acid (or sialic acid); *GalNAc*: *N*-acetylgalactosamine; *GalNAcT*: *N*-acetylgalactosamine transferase; *GD3s*: *GD3* synthase. Arrows represent the stepwise biosynthesis through glycosyltransferases.

### Figure S2

Binding and neuropathophysiological effects of mouse anti-GM1 mAbs DG1 and DG2 at NMJs. (A) DG1 and DG2 effect in ex-vivo hemi-diaphragm (as described in Figure 2). Neither mAb bound in the *GalNAcT*<sup>-/-</sup> mouse, resulting in absence of a complement mediated loss of neurofilament. IgG, C3c and MAC deposition are shown as signal intensities, with NF loss quantified as area coverage (percentage) over the NMJ. (B) MEPP frequency at ex vivo WT and *GD3s*<sup>-/-</sup> hemi-diaphragm NMJs, following DG1 or DG2 incubation and the presence of NHS as complement source. At both the *GD3s*<sup>-/-</sup> and WT NMJs, only DG2 is shown to cause an increase in MEPP frequency. (C) Tissue processed for immunohistology following DG2 (left panel) and DG1 (right panel) incubation of the ex vivo *GD3s*<sup>-/-</sup> hemi-diaphragm. Following incubation in NHS, tissue was snap frozen and cryostat sections were immunostained to detect IgG, C3c and MAC deposition, and neurofilament (NF) presence. Only DG2 was detectable at the NMJ, and able to cause a complement mediated destruction of the NF, in contrast to DG1, as illustrated. Scalebars represent 60\_μm

### Figure S3

(A) Topical immunostaining in frozen diaphragm sections of WT, *GD3s*<sup>-/-</sup> and

*GalNAcT*<sup>-/-</sup> mice to show DG2 specificity for Gal(β1-3)GalNAc epitope of GM1 (as opposed to that of GD1b). DG2 binding is abolished in the WT and *GD3s*<sup>-/-</sup> by pre-incubation of the tissue in unlabelled CTB to saturate GM1. As a control, abolition of binding of DG1 (which is monospecific for GM1) is shown at the *GD3s*<sup>-/-</sup> NMJ following CTB incubation. DG2 binds no epitopes at the *GalNAcT*<sup>-/-</sup> NMJ. \* indicate a statistically significant (p<0.05) decrease in binding compared to non-CTB blocked tissue. **(B)** GD1b is present in the motor nerve terminal. MOG1 (anti-GD1b mAb) binds ex vivo WT hemidiaphragm NMJs, and following addition of NHS, causes a complement-dependent loss of neurofilament (NF). \* indicate a statistically significant increase in IgG, C3c or MAC deposition or a decrease in NF coverage of the NMJ compared to Ringer's exposed control tissue. **(C)** Graph: MOG1 staining, in contrast to DG2, is not blocked by CTB, confirming Gal(β1-3)GalNAc epitopes of available GD1b in tissue are not binding DG2 (\*, p<0.05). Images: Illustrative example of the topically stained diaphragm sections, as analysed and quantified in the graph. Pre-incubation of tissue with CTB (unlabelled) abolishes DG2 staining, but has no effect on MOG1 intensity over the NMJ. **(D)** The immunopathological effects of DG2, as manifested by C3c and MAC deposition over NMJs (left panels), is blocked by CTB (middle panels) and also absent in control tissue (right panels). Scalebars represent 60\_μm.

#### **Figure S4**

**(A)** FACS analysis of immunostained *C.jejuni*. CTB binds to strain O:19, which bears a 50:50 ratio of GM1 and GD1a mimicking LOS. CTB does not bind negative control strain O:3, which lacks the GM1-mimicking LOS. **(B)** Strain O:19 GD1a-mimicking LOS is confirmed by MOG35 binding, and was used to determine the ability of DG1 to bind GM1-like LOS in the presence of GD1a-like LOS. Binding studies were performed in live versus dead (UV irradiated or PFA fixated bacteria). DG1 binds strain O:19 bacteria, including killed bacteria. MOG35 was also able to bind the killed bacteria.

#### **Figure S5**

**(A)** MEPP frequency at the ex vivo WT hemidiaphragm NMJ, following pre-incubation with DG1 and in subsequent presence of NHS as complement source. Only pre-treatment

of tissue with neuraminidase is able to induce a DG1- and complement-dependent increase in MEPP frequency. **(B)** Reconstructed confocal microscope images of MOG35 binding at *GD3s*<sup>-/-</sup> ex vivo triangularis sterni NMJs. MOG35 binds with a strong axonal deposition over the NMJ (left panel), which is abolished by neuraminidase treatment to remove GD1a (right panel). **(C)** Illustrative example of DG1 binding in the *GD3s*<sup>-/-</sup> triangularis sterni following neuraminidase treatment. Staining is specific to the axon and intense over the pre-synaptic region of the NMJ (left panel). Neuraminidase treatment followed by CTB incubation prior to DG1 blocks DG1 binding (right panel), proving DG1 binding is specific for GM1. **(D)** Effect of neuraminidase on CTB pre-incubated tissue. Ex vivo *GD3s*<sup>-/-</sup> triangularis sterni preparations and quantification of IgG fluorescent intensity over the NMJ. DG1 binds neuraminidase-treated NMJs, but this binding is reduced (\*p<0.05) when CTB is applied to tissue prior to neuraminidase treatment, thus saturating native GM1. DG2 is able to bind to a similar level of intensity at NMJs of both neuraminidase and CTB pre-saturated tissue. Scalebars represent 20\_μm.

### Figure S6

**(A)** Effect of cholesterol depletion on DG1 and MOG35 mAb and CTB binding intensity on PC12 cells. No increase in binding intensity was seen for any ligand, as assessed by FACS analysis. **(B)** Effect of PI-PLC removal of GPI anchored proteins in PC12 cells. Reduced Thy-1 binding signifies removal of a proportion of GPI anchored Thy-1 (positive control). An increase in DG2 and MOG35 fluorescent intensity was observed following PI-PLC treatment, however DG1 binding remained negligible (Y axes have been adjusted for clarity). **(C)** Confocal images of ex vivo triangularis sterni NMJs from WT mice, demonstrating abundance of the GPI anchored protein CD59 (top left panel). PI-PLC treatment removes this protein and abolished staining (top right). MOG 35 staining has an axonal profile (bottom left), but following PI-PLC treatment the staining becomes diffuse indicating exposure of new GD1a epitopes (bottom right). Scalebars represent 20\_μm.

1. Svennerholm, L. 1994. Designation and schematic structure of gangliosides and allied glycosphingolipids. *Prog. Brain Res.* **101**:XI–XIV.